Picosecond Phase Grating Spectroscopy of Hemoglobin and Myoglobin: Energetics and Dynamics of Global Protein Motion†

Lynn Richard, Laura Genberg,‡ John Deak, Hui-Ling Chiu, and R. J. Dwayne Miller*

Department of Chemistry and Institute of Optics, University of Rochester, Rochester, New York 14627

Received February 13, 1992; Revised Manuscript Received July 7, 1992

ABSTRACT: Phase grating spectroscopy has been used to follow the optically triggered tertiary structural changes of carboxymyoglobin (MbCO) and carboxyhemoglobin (HbCO). Probe wavelength and temperature dependencies have shown that the grating signal arises from nonthermal density changes induced by the protein structural changes. The material displaced through the protein structural changes leads to the excitation of coherent acoustic modes of the surrounding water. The coupling of the structural changes to the fluid hydrodynamics demonstrates that a global change in the protein structure is occurring in less than 30 ps. The global relaxation is on the same time scale as the local changes in structure in the vicinity of the heme pocket. The observed dynamics for global relaxation and correspondence between the local and global structural changes provides evidence for the involvement of collective modes in the propagation of the initial tertiary conformational changes. The energetics can also be derived from the acoustic signal. For MbCO, the photodissociation process is endothermic by 21 ± 2 kcal/mol, which corresponds closely to the expected Fe–CO bond enthalpy. In contrast, HbCO dissipates approximately 10 kcal/mol more energy relative to myoglobin during its initial tertiary structural relaxation. The difference in energetics indicates that significantly more energy is stored in the hemoglobin structure and is believed to be related to the quaternary structure of hemoglobin not present in the monomeric form of myoglobin. These findings provide new insight into the biomechanics of conformational changes in proteins and lend support to theoretical models invoking stored strain energy as the driving force for large amplitude correlated motions.

One of the key issues in understanding protein dynamics is the underlying mechanism for structural changes that are integral to the protein's function. These structural changes often involve large amplitude correlated motions that require the concerted action of a large number of atomic degrees of freedom. In this regard, heme proteins are one of the most important protein systems exhibiting large amplitude correlated structural changes. For hemoglobin and myoglobin, the changes in conformation are triggered by the binding and dissociation of small ligands, such as O_2, NO, and CO (Antonini & Brunori, 1971). The CO ligated form is particularly valuable in that it exhibits virtually unit quantum efficiency for photodissociation (Gibson & Ainsworth, 1957) with recombination occurring much slower than the ensuing ligated (oxy) to deoxy tertiary structural changes (Murray et al., 1988b; Anfinrud et al., 1989; Petrich et al., 1988). This feature of heme proteins makes it possible to optically trigger the structural changes and follow the structural relaxation pathway with optical probes which are sensitive to different aspects of the protein's motion. The ability to optically initiate the structural changes, and the detailed structural information available for these molecules from X-ray diffraction studies, makes them ideal model system for studying the relationship between protein dynamics and function. Another important aspect of heme protein dynamics is that the structural changes can be followed at both the tertiary and quaternary level. For example, in the case of hemoglobin, the changes in the tertiary structure of the monomer heme proteins alter the forces at the $\alpha\beta$ interface of the hemoglobin tetramer. The cumulative actions of the tertiary changes ultimately lead to the R → T quaternary structural change that controls the O_2 binding efficiency of hemoglobin. The state of ligand occupancy is communicated to the adjacent subunits through the tertiary structural changes. This communication link is the heart of the mechanism of allosteric control of protein function (Monod et al., 1965; Perutz et al., 1987; Gelin & Karplus, 1977). Thus, understanding the correlated conformational changes of heme proteins is important in understanding both protein dynamical responses and molecular cooperativity.

There have been numerous mechanisms proposed for heme protein processes. These models all invoke the release of stored potential energy, with the heme ligation site(s) as the focal point for the forces displacing the atoms to their new positions. The major distinguishing features of these various models are the length scale over which the forces act and the multiplicity of pathways along the structure coordinate.

One of the most detailed models for the conformational changes was developed by Perutz and will be referred to, herein, as the localized strain model (Perutz, 1970; Perutz et al., 1987). This model originated from the static differences in structure between oxy and deoxy heme proteins. Specifically, the doming of the heme following ligand dissociation was viewed as creating a force which causes the proximal histidine to tilt. This strain is localized over dimensions corresponding to one amino acid residue. The strain spatially displaces the force to the EF α-helix, which eventually drives the helix to its deoxy position. The overall structural changes occur through the propagation of the atomic displacements in a sequential manner, analogous to the sequential falling of dominoes. An important feature of this model is that the whole process is orchestrated by the specific structure of the protein. When a stimulus acts on the system, the energy released during the course of the protein's response to the

† This research was supported by the NIH (1 R01 GM41909-01A1) and an NSF Presidental Young Investigator Award (R.J.D.M.). R.J.D.M. is the receipient of an A.P. Sloan Fellowship and a Camille and Henry Dreyfus Teacher–Scholar Award.

* Author to whom correspondence should be addressed.

‡ Present address: Life Sciences Research Laboratory, Eastman Kodak Company, Rochester, NY 14650.

0006-2960/92/0431-10703$03.00/0

stimulus can cause motion in only one direction as the other motions are sterically hindered.

A paradigm that incorporates the strain model, but includes a dynamic sampling of the different potential energy minima in the protein's potential energy surface, has been described within the conformational substate model (Austin et al., 1975; Frauenfelder et al., 1991). Each minima in this model corresponds to a slightly different conformation. The system has a certain dwell time in each conformation that depends on the effective barrier separating different conformations. The protein relaxation is characterized by nonexponential kinetics, which reflects the thermally activated Brownian motion of the protein through a distribution of distinct conformational intermediates along a complex relaxation coordinate. The main distinction of this conformational substate model from the localized strain model is that it includes multiple pathways for the propagation of the structural changes.

The above models that the potential energy gradients that drive the system response are localized over some length scale. This assumption requires that the protein be flexible over the same length scale. At the opposite extreme, the protein may respond as a rigid body (on the relevant time scale of the structure transition). In this case, the forces are redistributed over the entire protein structure. In this event, the doming of the heme following ligand dissociation would lead to the collective displacement of a large number of atoms. The propagation of the structural changes would then best be described by a superposition of low-frequency spatially extended modes or collective modes of the protein. Evidence for these types of motions in proteins have been obtained from both experimental studies (Painter et al., 1982; Cusack & Doster, 1990) and analytical studies (Brooks & Karplus, 1985; Seno & Gō, 1990). The frequency range for collective modes is 1–50 cm^{-1}, which corresponds to picosecond time scales for the atomic displacements associated with these modes. In order for a net change in structure to occur through collective modes, the segments of the protein at the focus of the forces for the motion must be more rigid than the adjacent areas. In the case of heme proteins, the α-helical sections forming the heme pocket are more rigid than the corners (Seno & Gō, 1990). If these sections are sufficiently more rigid than the corners, then the doming of the heme with ligand dissociation could lead to a collective displacement of the atoms onto the global energy minimum corresponding to the deoxy structure. Such a collective displacement of atoms would represent the most efficient mechanism possible for the functionally important motions of the protein.

The tertiary and quaternary conformational changes of heme proteins, activated by changes in the state of ligation at the heme, offer an ideal response function for understanding deterministic protein motion. The above models for the heme protein response function vary in the length scale over which the forces act and the multiplicity of the functionally relevant pathways. In order to understand the protein's dynamical response, the length scale over which the induced potential energy gradient is delocalized needs to be determined. This can be accomplished by studying the protein dynamics with probes which are sensitive to different length scales of the protein motion. In addition, the relative importance of each phase of the structural relaxation can be determined from a study of the energetics. The study of the protein motion with probes sensitive to different length scales, along with the energetics for the motion, should enable a distinction between the localized strain, conformational substate, and collective displacement models for the heme protein structural transitions. All three descriptions of the atomic displacements probably operate to some degree. The issue is which mechanism is dominant.

Herein, we describe the use of phase grating spectroscopy to address the above issues with respect to the optically triggered tertiary structural changes of MbCO and HbCO. Due to the interferometric nature of this method, it is highly sensitive to density changes. Density changes can occur either through material displacement caused by the protein's own motion or through thermal expansion subsequent to energy release as the protein's structure evolves to the lowest energy configuration. These density changes are holographically imaged into a diffraction grating to give a real time view of the protein's motion and the energetics involved in undergoing this motion. The two different contributions to the density changes (conformational and energetics) can be independently determined, as will be elaborated below. In addition, the various models for allosteric regulation rely on the relief of built-in strain in the protein structure to drive the conformational changes. Phase grating spectroscopy provides a direct measurement of material strain and released strain energy, two fundamental parameters needed to understand the mechanics.

EXPERIMENTAL PROCEDURES

The experimental setup used a Q-switched and mode-locked Nd^{3+}:YAG laser operating at 500 Hz to provide excitation and probe pulses at 532 nm and 1.064 μm for the grating pulse sequence, as previously described (Genberg et al., 1989, 1991). The only major modification in the experimental setup was that probe pulses at both 532 nm and 1.064 μm were present simultaneously so that the absolute diffraction efficiencies could be measured at the two wavelengths under identical excitation conditions. The excitation spot sizes were 200 μm, and the probe spot sizes were 160 μm. The excitation pulse energy was typically less than 500 nJ for the lowest excitation studies ($\leq$2 mJ/cm^2) to ensure that only one photon process contributed to the signal. This excitation level corresponds to less than 10% bleach of the ground-state population for the focusing conditions used. In the studies where an excitation dependence was conducted, the excitation intensity is reported in the figure. Absolute diffraction efficiencies were determined by measuring the probe intensity before the sample and the diffracted signal with the same photodiode. To correct for differences in optimized Bragg angle and beam parameters for the two wavelengths studied, the absolute diffraction efficiencies were referenced to the signal from a pure acoustic grating provided by the deoxy form of the protein under study. Depending on the exact excitation conditions, variations of 2–4 were observed in the absolute diffraction efficiencies while the ratios at the two probe wavelengths were reproducible to within 20%.

The hemoglobin samples were prepared using standard techniques from fresh whole blood (Antonini & Brunori, 1971). This method prepared the oxy derivative. If the CO form was desired, the CO was passed over the solution until the UV–visible spectra indicated complete conversion. The preparation of deoxy-Hb involved extensive flushing of met-Hb with nitrogen and subsequent reduction with a molar excess of sodium dithionite. The myoglobin (Sigma, horse heart, type III) was dissolved in 100 mM Tris buffer, pH 7, and was reduced anaerobically using a slight molar excess of sodium dithionite. If the CO form was desired, the CO was passed over and the sample readily converted. For the deoxy samples,

special care was taken to ensure that oxygen was removed from the sample cells. The procedure included the use of sealed flasks and a nitrogen purged sample cell fitted with septums that enabled sample transfer under nitrogen. Heme octapeptide was prepared from horse heart cytochrome *c* according to the procedure of Kraehenbuhl et al. (1974) and used in its reduced CO form.

The protein samples were housed in an airtight rotating cell to avoid an accumulated thermal effect and to ensure that successive laser shots encountered a fresh sample. Small path lengths were used, on the order of 250 μm, to avoid excess scatter from bubbles that otherwise were spun into the beam sampling region with longer cell path lengths. The small path lengths necessitated the use of concentrations on the order of 1–3 mM in order to ensure adequate signal to noise ratios. For the temperature dependence studies, a flowing cell design was used with a path length of 1 mm which was cooled with a 50% v/v mixture of ethylene glycol and water from a temperature-controlled bath (Neslab Endocal RTE-100). The flow was obtained by using a Rainin Rabbit peristaltic pump with a flow rate of approximately 10 mL/min. The width of the cell was reduced to 1 mm so that this flow was sufficient to ensure an adequate sample turn over between laser shots. The temperature was measured with a thermocouple readout combination (Omega DP81-T) that was fitted with a 20 gauge needle. This needle was fitted through a septum port adapter in the cell so that the temperature could be measured directly. Due to the larger path lengths of this cell, sample concentrations were on the order of 1 mM.

The energetics were determined by going to a 75% glycerol/25% water solvent. The protein samples were prepared as previously described with the exception that the solutions were made up from stock solvent, and the conversion to the carboxy form of the protein took several hours of stirring under CO to ensure the protein had completely converted. The samples and stock solvent were always kept in sealed vessels, and transfers were made with needle stock to avoid the pick up of water from the atmosphere. The deoxy form of the protein was used as the reference for 100% deposition of the absorbed photon energy. The optical density of the deoxy sample was adjusted to be as close as possible to the carboxy heme. Calibration curves were made as a function of optical density to correct for any small differences in the optical density between the sample and reference. The optical densities were measured directly in the rotating cell used to make the measurements and the signal scaled according to the calibration curve. For most of the measurements, the optical densities were within a 5% difference such that this procedure was unnecessary. The excitation conditions were also monitored and kept to within a 5% difference between the excitation pulse energies used to determine the signal level from the deoxy reference and the carboxy heme. A minimum of five independent measurements were made in the evaluation of the energetics, and a minimum of three measurements were made for all other reported measurements.

RESULTS AND DISCUSSION

Structural Relaxation Dynamics. Studies using phase grating spectroscopy have been performed on the carboxy/deoxy structural transition for both MbCO and HbCO using 532-nm excitation pulses. Excitation into the Q-band at 532 nm dissociates the CO ligand in less than 100 fs (Petrich et al., 1988; Anfinrud et al., 1989) with the formation of a deoxy-like species with the iron partially out of the heme plane within 350 fs (Martin et al., 1983). The current studies are concerned

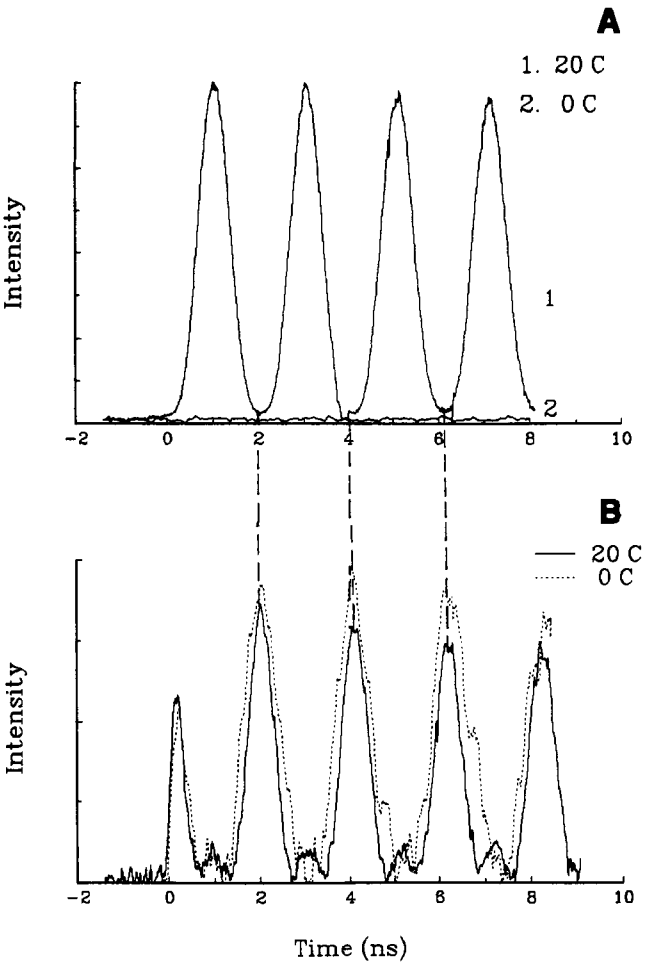

FIGURE 1: Temperature dependence of phase grating studies. (A) Deoxymyoglobin reference for pure thermal acoustic reponse. The lower curve is data collected at 0 °C. The signal is reduced by a factor of 140 near the zero thermal expansion point of water. (B) MbCO results with excitation pulse conditions of 1 mJ/cm². The dotted vertical lines are to illustrate that the acoustics driven by the protein tertiary structural changes are 180° out of phase with the pure thermal acoustic response exhibited by the deoxymyoglobin. The dashed curve is at 0 °C under the same excitation and probe conditions.

with the initial tertiary structural relaxation from this optically prepared nonequilibrium structure. Experimental phase grating studies for carboxymyoglobin (MbCO) are shown in Figure 1. These data were collected using a grating excitation angle (θ_{ex}) of 10° and an off-resonant probe at 1.064 μm. The controls for these studies are the deoxyheme protein analogues. The excited state lifetime of both deoxymyoglobin and deoxyhemoglobin is less than 3.2 ps (Petrich et al., 1988; Huppert et al., 1977). The fast relaxation of the deoxyheme excited state prepares a highly vibrationally excited ground state. The subsequent energy thermalization process to the surrounding water occurs in less than 22 ps (Genberg et al., 1987; Miller, 1991). This time scale is much faster than this grating acoustic period such that the deoxy heme studies serve as a reference for a pure, impulsive, thermal grating response.

The results shown in Figure 1A for deoxymyoglobin give the expected results for this limit, i.e., the first maximum in the signal is at half an acoustic cycle after the excitation pulse sequence ($t = 0$) with nearly 100% signal modulation at the acoustic period (Nelson et al., 1980; Genberg et al., 1989). The results shown in Figure 1A agree with earlier studies of the ferric heme proteins (Genberg et al., 1987, 1989). The only difference is that the magnitude of the slow nanosecond

relaxation component is more than a factor of 2 smaller in the present study and is only discernible under higher excitation conditions.

Figure 1B shows the results for MbCO. In comparing the MbCO results to the deoxymyoglobin control, the most striking feature of the data is that the acoustics appear phase shifted by 180°. In addition, the rise time of the acoustic signal from MbCO is much faster than the thermally driven acoustic response. The magnitude and temporal response of the acoustics are significantly different from that expected for a pure thermal response. These findings suggest that the observed acoustics arise from density changes associated with the optically triggered tertiary structural changes. In the event the protein conformational changes are coupling to the hydrodynamics, the acoustic mechanism should be nonthermal in nature. This feature of the acoustics was verified by studying the protein-driven acoustics near the zero thermal expansion point of water. At this temperature, small changes in temperature do not lead to a significant change in density. The amplitude of the thermal acoustics does not go completely to zero because the protein contributes to the material thermal expansion and does not go through a zero thermal expansion point. However, the decrease in the acoustic signal is sufficiently large near 0 °C that the thermal acoustics are essentially eliminated. The thermal grating signal from deoxymyoglobin was found to be reduced by a factor of 140 at this temperature (Figure 1A, lower curve). In contrast, the amplitude of the MbCO-driven acoustics remains nearly unchanged at this temperature relative to room temperature (Figure 1B, dashed curve). This result unambiguously demonstrates that the acoustics associated with CO photodissociation are nonthermal in nature. Herein, these acoustics will be referred to as the protein-driven acoustics.

A concentration dependence study was also conducted. The acoustic signal observed for MbCO was essentially identical over a concentration range from 3 to 0.3 mM. The only concentration-dependent effect observed was the increase in the magnitude of the reduction in the thermal acoustic amplitude in going from room temperature to the zero thermal expansion point of water at the lower concentrations. This observation is related to the protein's contribution to the material thermal expansivity. The acoustic wave speed can also be determined from the data shown in Figure 1. The acoustic wavelength (Λ) is given by the grating fringe spacing [$\Lambda = \lambda_{ex}/2 \sin(\theta_{ex}/2)$] and the acoustic period. The observed acoustic speed of sound is 1.5×10^5 cm/s, which is in excellent agreement with that expected for water. The lack of a concentration dependence and the excellent agreement of the acoustic period with the water wave speed demonstrates that the protein structural changes are coupling to the surrounding water.

The temporal dependence of the acoustics indicates that the protein motion is leading to a modulated density change which is 180° out of phase with the thermally driven acoustics. The most interesting new observation is that the protein motion appears to lead to density modulations capable of meeting the condition for Bragg diffraction in less than one-tenth of an acoustic period. This is much faster than that possible for $t = 0$ sinusoidal stress boundary conditions that occur in the conventional coupling of grating images to acoustic fields. However, it is possible that the protein-driven acoustics follow the normal impulse response and are beating against a population phase grating component. This possibility can be understood by examining the full expression for the grating diffraction efficiency in which both amplitude and phase contributions to the grating signal from population modulations are included. The complete grating equation is (Nelson et al., 1982a; Kogelnik, 1969; Siegman, 1977)

$$\eta = \exp(-\alpha d/\lambda_p \cos\theta_p)\left(\frac{2\pi d}{\lambda \cos\theta_p}\right)^2[(\Delta k_{ex})^2 + (\Delta n_{ex} + \Delta n_s)^2]G(w_{ex},w_p) \quad (1)$$

where θ_p is the probe Bragg angle, d is the grating thickness, α is the sample absorptivity at the probe wavelength (λ_p), $G(w_{ex},w_p)$ is a constant geometrical correction factor for Gaussian beams that depends on relative spots sizes (w) of the excitation and probe beams. The terms Δk and Δn refer to peak-null variations in the imaginary and real parts of the complex index of refraction, i.e., amplitude and phase grating components, respectively. The subscripts "ex" and "s" are used to define the spatial variations in k and n that arise from excitation-induced changes in the population and material strain, respectively. The acoustic strain only affects the phase grating amplitude and can show up as a cross term with the population phase grating term Δn_{ex} (Nelson et al., 1982a). In this case, the acoustics can lead to either a positive or a negative sinusoidal modulation of the grating signal at the acoustic period of the grating. Whether the acoustic modulation is positive or negative depends on the sign of the acoustic modulated index relative to the population term. Both positive and negative signal modulations have been observed.

In order to explain the observed grating signal, the acoustic strain would have to be opposite in sign and the same magnitude as the population phase grating component (i.e., $\Delta n_s = -\Delta n_{ex}$ in eq 1). This possibility needs to be considered as there will always be a small population phase grating contribution no matter how far off-resonance the probe is. Whether or not this explanation accounts for the observed acoustics depends on the magnitude of the population phase grating component at 1.064 μm relative to the acoustic component. The relative amplitude of the population phase grating component to the acoustic component was determined by studying the acoustics at two independent probe wavelengths under identical excitation conditions. By going to a resonant probe wavelength, the population phase grating component can be selectively increased by an order of magnitude over the acoustic component relative to the off-resonant case discussed. If the population phase grating component is comparable in magnitude to the acoustic component for off-resonant probes, then it should dominate the signal for resonant probes. In addition to this consideration, the relative magnitude of the population grating at different wavelengths can be independently determined if the spectroscopy is well characterized. It has previously been established that the dissociation of CO from MbCO leads to an absorption spectrum essentially identical to the equilibrium deoxymyoglobin spectrum in less than 30 ps (Petrich et al., 1988). Therefore, the equilibrium spectra of the carboxyheme proteins and their deoxy derivatives can be used to determine the magnitudes of the population phase grating components at different wavelengths, for times in excess of 30 ps following the excitation pulse sequence.

Probe wavelengths at 532 nm and 1.064 μm were used to evaluate the population phase grating component. The relative positions of the two probe wavelengths with respect to the absorption spectra of MbCO and deoxymyoglobin are shown in Figure 2A. As can be seen from this figure, the 1.064-μm probe is significantly off-resonance in comparison to the 532-nm probe for both deoxymyoglobin and MbCO. In contrast, the 532-nm probe wavelength is ideally suited for a maximum dispersive contribution from the induced spectral changes in

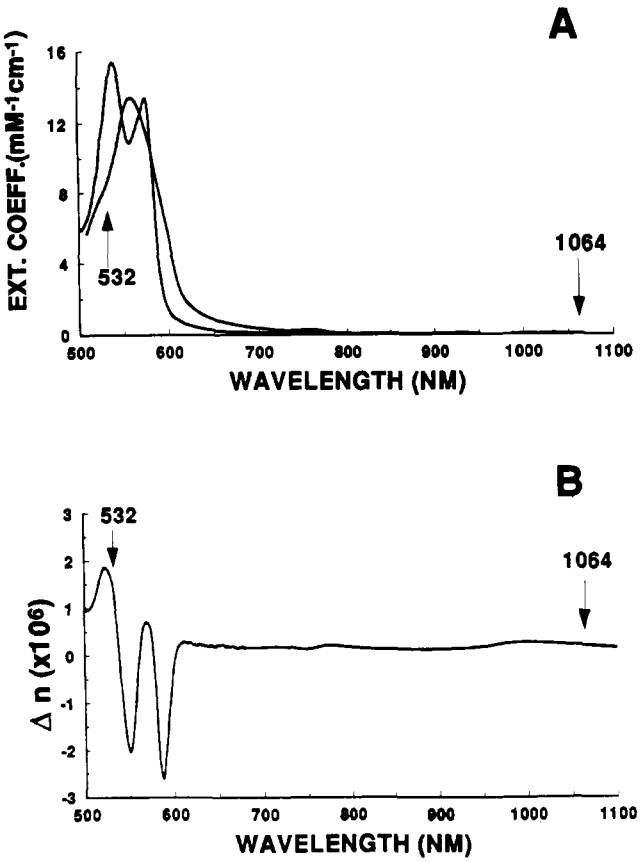

FIGURE 2: (A) Absorption spectra of MbCO. The arrows indicate the positions of the two probes used in these studies. (B) Kramers–Kronig calculation of the population phase grating component (Δn_{ex}) for MbCO as a function of wavelength based on the absorption difference spectrum of MbCO and deoxy-Mb. From this figure, it can be seen that the population phase grating component is at least 7 times larger at 532 nm relative to 1.064 μm.

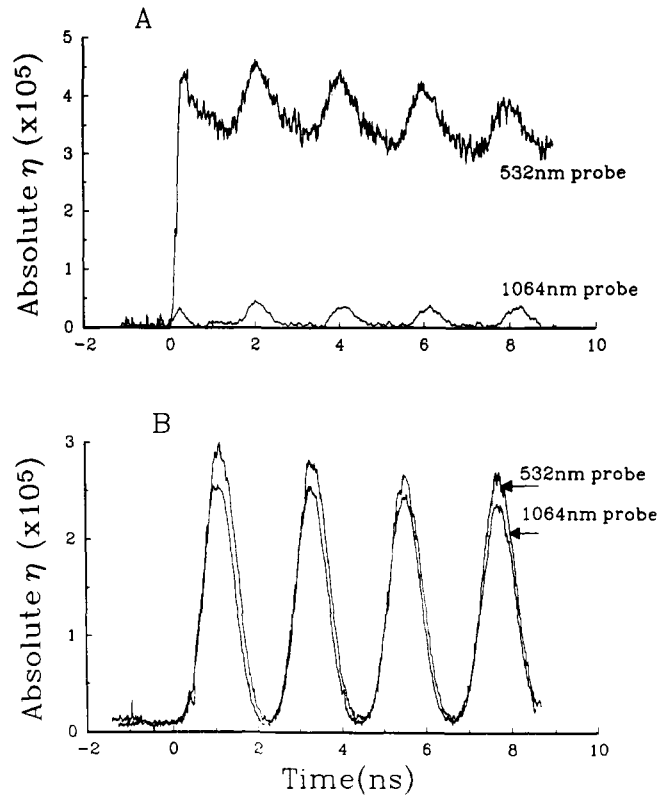

FIGURE 3: Probe wavelength dependence of the absolute diffraction efficiencies at excitation conditions of 1 mJ/cm^2. (A) MbCO. The ratio for the absolute diffraction efficiencies at the maxima is 9:1 for 532 nm relative to 1.064 μm under identical excitation conditions. The ratio of the acoustically modulated signal is 2.4:1. (B) Deoxymyoglobin. The ratio of the diffracted signal at 532 nm relative to 1.064 μm is 1.2. These data give the scaling with wavelength for a pure acoustic response.

the heme proteins. From the absorption difference spectrum, the relative magnitude of the population phase grating component at 1.064 μm and 532 nm can be determined from a Kramers–Kronig analysis (Nelson et al., 1982a; Eichler et al., 1986), i.e.

$$\Delta n_{ex}(\omega) = \frac{c}{2\pi} P \int_{-\infty}^{\infty} \frac{\Delta\alpha(\omega')\, d\omega'}{\omega'(\omega' - \omega)} \qquad (2)$$

where $\Delta\alpha$ is the optically induced change in absorptivity as a function of the optical radial frequency (ω). The Kramers–Kronig (K–K) integral for the population phase grating component was evaluated on the basis of the absorption difference spectrum for MbCO and deoxymyoglobin shown in Figure 2A with contributions from 250 to 1200 nm included in the calculation. The Cauchy principle value of the K–K integral was determined using the numerical method described by Chan and Page (1983). The calculated change in index of refraction for the population phase grating component from this analysis is plotted in Figure 2B. The absolute magnitudes of the index of refraction changes were calculated using the experimental conditions corresponding to Figure 1.

The most important consideration of this analysis is the relative magnitudes of the population phase grating component for the on-resonance and off-resonance case. The population phase grating component increases by more than a factor of 7 in going from 1.064 μm to 532 nm [$\Delta n_{ex}(532)/\Delta n_{ex}(1.064) > 7$]. The determination is near the signal to noise limit in the infrared region. A separate analysis based on assigned line shapes and oscillator strengths of the heme optical transitions (Eaton et al., 1978; Leone et al., 1987) found that the population phase grating component is more than 10 times larger at 532 nm (Genberg, 1990). Taking into account the quadratic scaling of the grating diffraction efficiency and wavelength dependence on the phase retardation, this change in dispersive contributions from the heme would amount to more than a factor of 200 increase in the diffraction efficiency from the population phase grating component at 532 nm relative to 1.064 μm (eq 1). The large difference in signal level from this grating contribution at the two probe wavelengths enables a determination of the relative importance of the population phase component at 1.064 μm.

The results from the probe wavelength study are shown in Figure 3. The top curve in Figure 3A shows the results observed for MbCO under low excitation conditions using a resonant 532-nm probe. As opposed to the 1.064 μm studies, the acoustic oscillations are now clearly superimposed on top of a population grating that develops due to the different optical properties of MbCO relative to Mb at 532 nm. At this probe wavelength, there are both significant amplitude (Δk_{ex}) and phase (Δn_{ex}) components to the population grating. The population grating relaxes with CO recombination at the heme site on an approximately 100-ns time scale. The observed population grating decay as well as independent pump/probe studies at 532 nm (Genberg, 1990) are in agreement with earlier studies which have well documented the MbCO and HbCO recovery kinetics (Henry et al., 1983; Murray et al., 1988). For the 10-ns time scale shown in Figure 3 for MbCO, the population grating appears as an approximately constant baseline offset after $t = 0$. Beyond this difference, the acoustics

are virtually identical in form to the results obtained at 1.064 μm.

The most important feature of this study is the magnitude of the absolute diffraction efficiencies. The signal obtained for the 1.064-μm probe studies under identical excitation conditions gives an absolute diffraction efficiency only 9 times less than the resonant 532-nm probe case (compared to the expected ratio for a population grating of 200:1). This ratio does not take into account the amplitude component to the grating signal at 532 nm which will reduce this ratio even further. Even without this consideration, it is apparent that the signal level at 1.064 μm is over an order of magnitude too large relative to the 532-nm probe case to be explained as an acoustic response beating against a population grating offset.

The absolute diffraction efficiency from the protein-driven acoustics was further referenced to the thermally driven acoustics exemplified by deoxymyoglobin, as a control for the pure acoustic response. This comparison also corrects for differences in the absolute diffraction efficiency at the two probe wavelengths that might arise from the different Gaussian beam parameters and probe attenuation. This study is shown in Figure 3B for deoxymyoglobin at the same optical density at 532 nm as the MbCO study shown in Figure 3A. In this case, the diffraction efficiency is found to be 1.2 times larger at 532 nm relative to the 1.064 μm case. This observed signal scaling in Figure 3B gives the pure acoustic grating dependence on wavelength for this grating configuration.

The difference in absolute diffraction efficiency at 532 nm and 1.064 μm for the pure acoustic response is close but not identical to that for the MbCO studies. However, as mentioned above, in the case of MbCO there is a long-lived population grating which is absent in the deoxymyoglobin studies. The population grating signal at 532 nm is comprised of both amplitude and phase grating components. The amplitude grating component is not subject to acoustic modulation as this would require a density dependent spectral shift which has been shown to be negligible except at liquid helium temperatures involving very narrow absorption line shapes (Miller et al., 1984). It is for this reason that there is no acoustic contribution included in eq 1 for the amplitude contributions. The amplitude grating component needs to be subtracted from the diffraction efficiency to make a comparison to the pure acoustic case.

The exact ratio of the amplitude and phase grating components at 532 nm was determined by selectively increasing the magnitude of the thermally driven acoustics and underlying thermal grating. This was accomplished by increasing the excitation intensity, which results in an increase in the fraction of deoxymyoglobin relative to MbCO. The deoxymyoglobin fraction created through CO photodissociation at the leading edge of the excitation pulse is capable of absorbing several photons sequentially during the excitation pulse duration. This sequential photon absorption process, through population cycling of the short-lived deoxymyoglobin excited state, has been characterized previously (Greene et al., 1978). This effect leads to an increase in the amount of energy thermalized without changing the population ratio of MbCO to Mb or the amplitude of the protein-driven acoustics. The general form of the thermally driven acoustic contribution to the phase grating is $\Delta n_s = A(1 - \cos \omega_{ac} t)$, where A is the acoustic amplitude and ω_{ac} is the acoustic radial frequency. It is the amplitude (A) of the thermal acoustic response which is selectively increased by sequential multiphoton absorption. The thermal component is found to be opposite in sign to the nonthermal phase contributions. In the limit that the thermal grating amplitude is much larger than the protein-driven density changes, we can neglect the protein acoustics and $\eta_p \sim [\Delta n_{ex} - A(1 - \cos \omega t]^2$ for the fraction of diffracted light originating from nonthermal phase contributions. As the acoustic amplitude is increased, the acoustically modulated thermal grating amplitude will cancel the population phase grating twice per acoustic cycle for conditions in which $A \geq \Delta n_{ex}$ (and Δn_s from the protein). This frequency doubling effect results from the quadratic dependence of the diffraction process. For cases in which the thermal acoustics are opposite in sign to the other phase grating components, the maximum depth in thermal acoustic modulation determines the fraction of the signal which is phase in origin.

This experiment is shown in Figure 4 for MbCO. As seen from Figure 4, the maximum depth of thermal acoustic modulation is 25%, which gives the fraction of the diffracted signal from nonthermal phase grating components. Taking into account the fraction of the signal at 532 nm which comes from phase grating contributions, the ratio of the acoustic modulated phase grating diffraction efficiency at 532 nm relative to that at 1.064 μm for MbCO is found to be 1.5 [$\Delta n(532)/\Delta n(1.064)$]. This ratio is essentially in quantitative agreement with that found for the pure acoustic case and demonstrates that the signal observed for MbCO at 1.064 μm is predominantly an acoustic grating in nature. The comparison of the diffraction efficiencies from the acoustics at 532 nm and 1.064 μm under identical conditions shows that the total phase grating component ($\Delta n_{ex} + \Delta n_s$) is at most 40% larger at 532 nm relative to that at 1.064 μm. On the basis of the Kramers–Kronig analysis of the wavelength dependence of Δn_{ex}, the population phase grating is estimated to contribute less than 6% to the signal for $t > 30$ ps at 1.064 μm.

In addition to the MbCO studies, a dependence of the protein-driven acoustics on the globin structure surrounding the heme was conducted. These results are shown in Figure 5 for low excitation conditions using a 1.064-μm probe. The top panel shows the MbCO driven acoustics as a reference. Figure 5B gives representative results for carboxyhemoblogin (HbCO), while Figure 5C shows results for carboxyheme octapeptide which serves as a control for the carboxylated heme without the surrounding protein. The results are rather dramatic. In the case of HbCO, the heme protein exists in a quaternary structure in which it has long been postulated that the interfacial contacts between the subunits hinder the full development of the tertiary structural changes. This is observed. The amplitude of the protein driven acoustics, as indicated by the dotted lines in the figure, is 1.5–2 times smaller than the corresponding acoustic component for MbCO (Genberg et al., 1991). In addition, there is a much larger amplitude for the thermal grating contribution which is observed as an increase in the acoustic component in phase with the thermally driven acoustics. This leads to a doubling of the signal oscillations with the maximum signal observed for the acoustic component in phase with the thermally driven acoustics. This increase is related to the difference in energetics for HbCO relative to MbCO which will be discussed further below. In contrast to either MbCO or HbCO, carboxyheme octapeptide did not generate acoustics in phase with the protein wave. Only acoustic components corresponding to the thermal mechanism were observed. A small signal component is observed at $t = 0$ which rapidly decays. This signal component may arise from transitions originating from the short-lived excited state of deoxy-Mb or material strain which develops with the doming of the heme which rapidly collapses to the

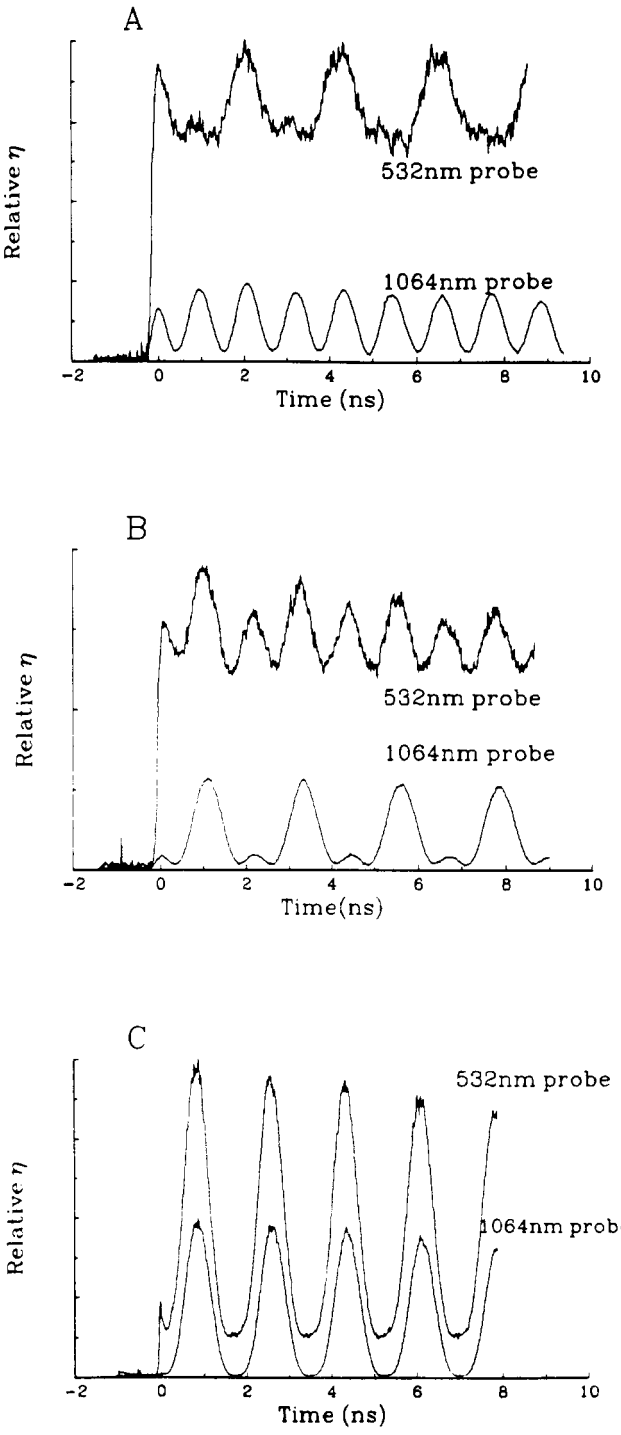

FIGURE 4: Power dependence on the acoustics for MbCO. The upper data sets are for a 532-nm probe, and the lower data are for 1.064-μm probes under identical excitation conditions. (A) Excitation conditions of 5 mJ/cm^2. (B) Excitation conditions of 10 mJ/cm^2. (C) Excitation conditions of 43 mJ/cm^2. As the excitation conditions are increased, the acoustic signal goes from being dominated by the protein-driven density changes to the thermal mechanism. The maximum depth of acoustic modulation of the signal by the thermal acoustics determines the contribution of the nonthermal phase grating relative to the amplitude grating contributions, which is found to be ~25% at 532 nm.

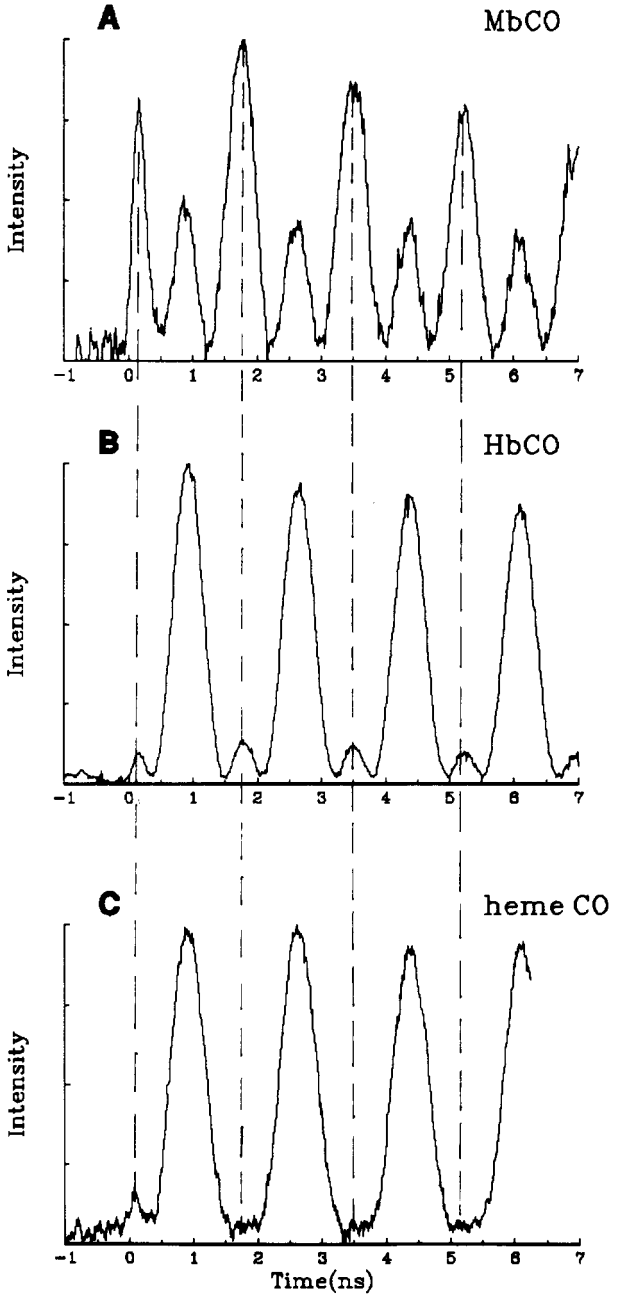

FIGURE 5: Grating dependence on protein for excitation conditions of 2.4 mJ/cm^2 at 532 nm and a 1.064-μm probe. (A) MbCO. The dotted lines depict the corresponding protein wave for MbCO relative to the other hemes. At this excitation level, the thermal wave is also visible. (B) HbCO. From absolute diffraction efficiency measurements, the protein wave in HbCO is 1.5–2 times smaller (η) than MbCO. (C) Carboxyheme octapeptide. There is a small signal near $t = 0$. No acoustics are observed other than the thermal mechanism. In the absence of globin surrounding the heme, there is no coupling to the fluid hydrodynamics.

original volume. The exact contributions from either source are not clear at the present time but can in principle be determined with better time resolution and a probe wavelength dependence. However, the most important observation is that the so-called protein-driven acoustics are not observed without the surrounding globin. This result and the temperature dependence demonstrate that the observed acoustics are originating from changes in strain in the globin following CO photodissociation and it is this induced strain in the protein which is coupling to the hydrodynamics.

The MbCO, HbCO, and carboxyheme octapeptide comparative studies show that the phase grating signal depends on the protein structure. From the dependence of the signal on the surrounding protein, quaternary structure, and the probe wavelength dependence of the absolute diffraction efficiency, it can be concluded that the grating signal at 1.064 μm is predominantly acoustic in nature for the CO-ligated heme proteins. This result means that the protein's optically triggered motion is forming a density grating. The density

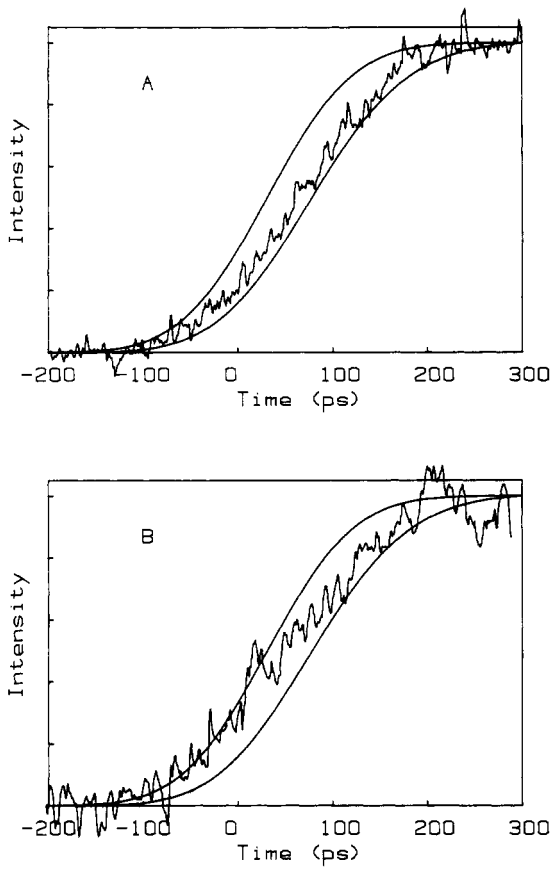

FIGURE 6: Short time dynamics for grating formation. (A) The grating rise time is shown for MbCO using 532-nm excitation and a 1.064-μm probe with a 2° angle between the excitation beams. The upper solid curve is the convolution of the grating excitation and probe pulses to an instantaneous rise time. The lower solid curve is for a 30-ps rise time. The noisy curve is the experimental data. (B) HbCO with the same details as in panel A. The rise times are $\leq$30 ps in both cases. The signal to noise ratio is not sufficient to extrapolate rise times less than one-quarter the pulse durations.

changes are nonthermal in nature, as shown by the studies at the zero thermal expansion point of water, and are attributed to optically induced changes in the protein tertiary structure with CO photodissociation. The density changes arise from the material displaced during the protein's structural transition from the carboxy to the deoxy tertiary structure. The coupling of this motion to the fluid hydrodynamics on the time scale observed would require a global change in protein volume, i.e., a net displacement of the exterior residues of the heme protein relative to the residues in the interior. This requirement is the same for any acoustic mode. The rise time of the grating is then directly related to the dynamics for the global protein motion. In essence, the protein motion is holographically recorded through the density changes it produces.

The rise time for the phase grating monitored at 1.064 μm is shown in Figure 6 for MbCO and HbCO. The data show a rise time of less than 30 ps. For the 130-ps pulses used in this study, 30 ps represents the limit in the temporal resolution. More recent studies using an IR up-conversion method to conserve picosecond time resolution have found that the rise time for MbCO has an effective time constant of less than 10 ps (Miller et al., 1992). The exact rise time is complicated by an optical Kerr effect that manifests itself with the shorter, higher peak power, pulses than the pulses used in this work. The higher time resolution studies need to be extended to include HbCO and further eliminate the Kerr effect to access the true protein dynamics. From the present study, the main conclusion is that the dominant phase of the global protein motion associated with the tertiary structure changes of myoglobin and hemoglobin occurs in less than 30 ps. There appear to be no significant slower relaxation components involved (i.e., >10%) in the protein motion from 30 ps to 10 ns at room temperature for both MbCO and HbCO. However, there are ~10% structural relaxation components on the nanosecond time scale at lower temperatures. The slower relaxation components are observable as a slight rise in the signal and a decrease in the depth of acoustic modulation (dashed curve in Figure 1B).

The finding that most of the global relaxation of the protein is complete in less than 30 ps is very significant as these dynamics are virtually identical to dynamical studies that probe local changes in structure near the vicinity of the heme pocket. In this regard, the most relevant series of investigations to the present discussion are the time-resolved Raman studies of the proximal histidine by Friedman and co-workers (Findsen et al., 1985a,b; Friedman, 1985). These studies have shown that the tertiary structural changes in the position of the proximal histidine are also complete within less than 30 ps. This study used 30-ps pulses and found that the deoxy frequency shift was fully developed for MbCO within that sampling window. This finding indicates that the proximal histidine rotates to its deoxy position on a 10-ps time scale or less. In order to test for the involvement of collective modes, one needs probes that are sensitive to atomic displacements over different length scales. The proximal histidine probes the local tertiary structural changes in the vicinity of the heme, which is the postulated focal point for the forces driving the oxy to deoxy structure changes. On the other hand, the phase grating studies probe the relative motion of the exterior of the protein. In both cases, the time scales for these different length scales of motion are approximately the same. In order for the dynamics to be similar, the exterior atomic displacements must be occurring at the same time as the interior of the protein, i.e., the atoms are moving together as a unit. The close correspondence of the dynamics of the global protein motion with the local changes in the vicinity of the heme gives evidence for the involvement of collective modes in the propagation of the structural changes. This conclusion was discussed earlier (Genberg et al., 1991) and is elaborated upon in the present work.

The observed dynamics for the changes in protein strain, alone, implicate the involvement of collective modes in the structural relaxation. Independent to these experimental studies, a normal mode analysis of MbCO and deoxymyoglobin found that more than 60% of the tertiary structural changes could be accounted for by the displacement of five spatially extended normal modes with frequencies ranging from 5 to 12 cm^{-1} (Seno & Gō, 1990). The experimentally observed rise time associated with the global motion of the protein is consistent with this frequency range. In addition, the fact that most of the global tertiary relaxation occurs within this same time frame is further consistent with the normal mode analysis and the concept that the initial phase of the protein relaxation can be defined as a superposition of collective modes.

It is interesting to note that the propagation of the tertiary conformational changes through collective modes is the most efficient mechanism possible for the structure transition. The evidence for the involvement of collective modes in propagating the tertiary structural changes does not rule out conformational substates playing a role in the full displacement of the atoms toward the global energy minimum associated with the deoxy structure. However, it does indicate that the potential energy

gradient would have to be extensively delocalized over the protein structure in order to couple to collective modes. This collective mode mechanism should be distinguished from the protein-quake model proposed by Ansari et al. (1985). Within this latter model, the protein relaxation was envisaged as a series of segmental motions of the protein that are statistically sampled through various conformations. The present evidence points to the excitation of various collective modes in phase by the impulsive doming of the heme following ligand loss. There appears to be no evidence at room temperature for a distribution of volume changes or quakes that would implicate conformational substrates. These would have shown up as slower rise time components in the initial grating formation and as shifts in the phase of the acoustics. However, as mentioned, there is evidence for small amplitude (<10%), slower relaxation components near the zero thermal expansion point of water. From these data, we infer that conformational intermediates to the fully equilibrated deoxy structure do not involve significant volume changes in the protein.

The rapid rise time in the protein-driven density changes relative to the thermal grating response is interesting to note in its own right. Previously, it has been proposed that nonthermal density changes in optically excited carboxyheme proteins arise from electrostriction effects (Westrick et al., 1990). For example, the breaking of a salt bridge in the protein changes the electric fields in the material. The polar water molecules reorient to the new fields and cause a net material contraction. However, electrostrictively driven sound fields exhibit approximately the same grating formation dynamics as thermally excited acoustics (Nelson et al., 1982b). The spatial distribution of charge would replicate the grating period to produce a stress acting over the length scale of the grating period. This effect gives $t = 0$ stress boundary conditions which match the grating wave vector. In this case, the rise time for density changes driven by electrostriction would be limited by the speed of sound for material displacement occurring over the dimensions of the grating fringe spacing. The spatial distribution of forces acting on the material are identical to the thermal mechanism in which the grating rise times are well documented to be on the order of half an acoustic cycle. For the grating geometries used in this study, these rise times are ~500 ps and not less than 30 ps. The observed dynamics for the protein-driven acoustics rule out this explanation.

In contrast, the phase grating studies indicate that there is a rapid change in density approximating a $t = 0$ sinusoidal strain boundary condition for the generation of the sound waves. The material displacement driven by the protein structural changes is responding to forces local to the heme. If the protein conformational changes involve a change in volume of the protein, the material displacement will mimic the dynamics of this motion. The protein's motion will displace both the surrounding water and sections of the protein matrix. The material displacement is arrested once the protein has undergone its full range of motion. This change in material density would be analogous to a time-dependent expansion coefficient in the thermal grating case, in which there is initially a very large value that rapidly goes to zero. If the material displacement driven by the protein motion goes to completion much faster than the grating acoustic period, then the acoustics will approximate a $t = 0$ sinusoidal strain boundary condition. In this case, the nonpropagating static component to the density grating would develop first, and the acoustics would respond to the strain induced stress in the material. This condition would lead to a 180° phase shift in the acoustics relative to the thermal case, as observed.

Similar mechanisms of high-frequency sound generation have been discussed previously. The use of light to create a $t = 0$ strain boundary condition for sound wave generation has been treated theoretically for photostriction phenomena in semiconductors (Dharamsi & Hassam, 1989). The predictions of this analysis for high-frequency sound generation are qualitatively in line with the above model for the protein waves, i.e., the rise time of the density changes depend only on the highest frequency acoustic phonon coupled to the lattice changes. In addition, there are experimental observations of rise times for index of refraction changes that are not limited by the speed of sound over the optically sampled volume but only by the highest frequency phonon coupled to the lattice distortion (Cho et al., 1990; Min & Miller, 1989, 1990).

The above model for the coupling of the protein motion to the hydrodynamics explains the general form of the observed acoustics. However, a detailed analysis of the mechanical coupling which includes the aqueous interface and the effect of the motion on the index of refraction needs to be developed to further test this model for the acoustic generation and obtain quantifiable parameters. For example, it is unclear whether the index of refraction changes are determined primarily by changes in the water density, protein density, or from the difference in these two contributions. If we assume the number density of oscillators is dominated by the water (which is the normal assumption based on percent composition of the medium), the index of refraction changes correspond to strain amplitudes of $\leq 10^{-4}$, which requires less than a 0.1-Å change in the effective radius of the heme proteins. However, a detailed theory for the density changes and index of refraction is needed to give reliable magnitudes for the changes in the global structure of the protein.

Energetics. There is little doubt that the protein has a very complex potential energy surface with multiple minima that correspond to different conformations at various points in the protein structure (Frauenfelder et al., 1991; Elber & Karplus, 1987). These different conformations are constantly being dynamically sampled through thermal fluctuations. Just how important these conformational substates are in the overall structural relaxation dynamics remains to be determined. Most of the evidence for conformational substates in the structural relaxation of heme proteins comes from temperature studies of the nonexponential geminate CO recombination dynamics (Frauenfelder et al., 1991). However, there is no direct connection between the barrier distribution for CO recombination inferred from these measurements and global relaxation of the protein. The barriers to CO recombination are not necessarily the same as those for the entire protein structure. In the case of CO recombination, the barriers are related to structural changes that modify the local potential energy surface in the vicinity of the heme and affect Fe–CO bond formation (i.e., the formation of a planar six-coordinate heme) and changes that influence CO diffusion to the heme site. In the case of global structure relaxation, the relevant variations in the potential energy surface include changes at the heme and at the protein/solvent interface. These potential gradients must be integrated over the entire protein structure in order to understand all the forces acting on the global structure coordinate.

A direct measure of the energetics relevant to the protein relaxation is needed to understand the effective driving forces for the protein motion. The energetics of the system response to ligand dissociation also provide an obvious criterion for

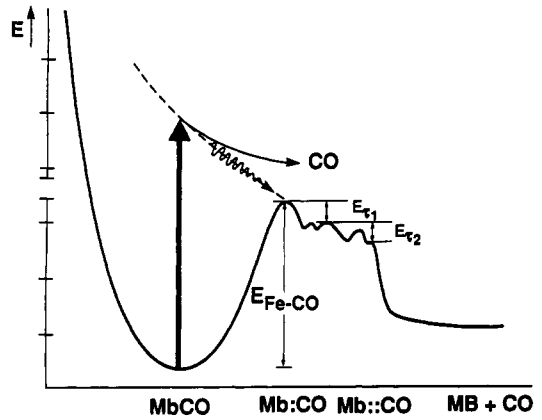

FIGURE 7: Energetics for optically triggered protein motion. This diagram shows schematically a one-dimensional slice through a complex multidimensional energy surface of the protein. Optical excitation prepares the system on a dissociative surface in which the Fe–CO bond is broken. The initially optically prepared state is a highly excited deoxy state and a CO physically trapped near the heme. The excited deoxy state rapidly dissipates the excess energy above that needed to break the Fe–CO bond ($E_{Fe\text{-}CO}$), and the protein undergoes relaxation toward its deoxy tertiary structure which also dissipates energy (E_{τ_1}). The next phase of the protein relaxation involves the diffusion of the CO out of the protein. Energy is released as the interactions between residues disrupted by the CO are reformed (E_{τ_2}) and the CO becomes solvated in the aqueous phase (E_s) to give the fully equilibrated deoxy heme protein.

determining the dominant mechanism for the structural relaxation. The mechanism that propagates the system furthest downhill in energy toward the global energy minimum corresponding to the final equilibrium structure should be classified as the dominant mechanism. The simultaneous measurement of the energetics and dynamics is unique in this regard as it should enable an unambiguous characterization of the relative importance of the various phases of the protein relaxation in the attainment of its final structure. For example, if conformational substates play an important role in the overall evolution of the system, the energetics should show a distribution of relaxation rates. In contrast, if the structural changes are propagated largely through the impulsive excitation of collective modes, then the energetics should show the majority of the energy dissipated during the rapid collective phase of the motion.

The energetics of the optically induced structural changes are shown schematically in Figure 7. There is the Fe–CO bond enthalpy, the amount of absorbed photon energy above the bond energy, and the energetics of the triggered protein relaxation to consider. Optical excitation at 532 nm places the heme on a dissociative electronic surface that breaks the Fe–CO bond. A certain fraction of the absorbed photon energy goes toward breaking the Fe–CO bond, and the excess energy above this amount will be rapidly dissipated into the bath (Lingle et al., 1991; Petrich et al., 1987; Miller, 1991). The rapid dissipation of this excess energy is equivalent to the nonradiative relaxation of the short-lived deoxy heme protein excited states and contributes to the rapid rise time in the thermal grating. The subsequent relaxation of the nonequilibrium protein structure toward the deoxy structure will also dissipate energy into the bath. The amount of energy dissipated and the dynamics for the energy relaxation will depend on the energy difference between the carboxy and deoxy tertiary structure and the barrier distribution between conformational substates that may act as real intermediates in the structural relaxation.

As can be appreciated from Figures 1 and 5, the problem in attaining information on the heme protein energetics in the

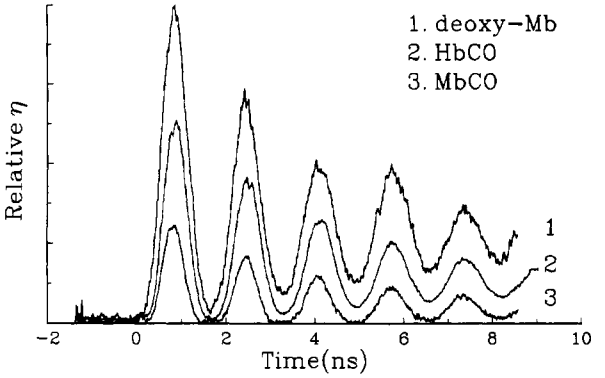

FIGURE 8: Phase grating studies of the protein relaxation energetics in 75% glycerol/25% water using 532-nm excitation and a 1.064-μm probe. The results are representative of at least five scans with excitation conditions less than 2 mJ/cm². Curve 1 represents the diffracted signal for the deoxy heme protein under the same experimental conditions. The diffracted signal level was the same for both deoxy-Mb and deoxy-Hb under the same conditions. The deoxy heme serves as the reference for complete dissipation of the absorbed photon energy. Curve 2 is for HbCO, and curve 3 gives the results for MbCO. From the comparison of MbCO and HbCO, it is apparent that more energy is thermalized within the same time frame for HbCO than MbCO. The decay of the acoustic modulation is due to acoustic attenuation in this viscous medium.

present study is that the grating has a substantial contribution from protein volume changes and is not exclusively a thermal grating. This is especially true for MbCO, where the protein-driven density changes dominate the signal. This problem was overcome by going to a 75% glycerol/25% water solvent system. The advantage of the glycerol/water solvent is that the thermal expansion coefficient is an order of magnitude larger than water. With this solvent system, the thermal phase grating components dominate the signal, allowing a fairly straightforward determination of the energetics. In addition, this is the same solvent system used by Frauenfelder and co-workers to establish the existence of conformational substates in heme proteins, and a great deal of effort has been made in making a correlation between the protein dynamics in this medium and physiological aqueous conditions (Ansari et al., 1985).

The results from this study are shown in Figure 8 for MbCO and HbCO using 532-nm excitation and a 1.064-μm probe. The results shown in Figure 8 make a direct comparison of the thermal grating dynamics for MbCO and HbCO with their deoxy analogue under the same conditions. The deoxy heme proteins serve as a reference for the case in which all the absorbed photon energy is dissipated into the aqueous bath with a time constant less than 22 ps. For MbCO, the protein wave is still present, but the thermal grating response now dominantes the signal. As can be seen from Figure 8, the amplitude of the thermal phase grating is significantly less for MbCO than the deoxymyoglobin due to the fact that some of the energy has to go into breaking the Fe–CO bond. The difference in energy can be determined from the difference in signal amplitudes of the deoxy-Mb reference and the MbCO results, i.e.,

$$\Delta E = [1 - (\eta_{MbCO}/\eta_{Mb})^{1/2}]E_{h\nu} \quad (3)$$

A detailed comparison of several samples in which the experimental conditions were kept constant and use of calibration curves to correct for optical density differences between the deoxymyoglobin reference and MbCO found that the difference in energy is 21 ± 2 kcal/mol. This result can be inferred from Figure 8, in which the thermal grating amplitude of MbCO is slightly more than one-quarter the

deoxy-Mb reference. This means that just more than half the 532-nm photon energy (54 kcal/mol) is dissipated.

This amount of energy corresponds very closely to the expected value for the Fe–CO bond enthalpy. Previous studies have estimated the bond energy to be 25 kcal/mol (Antonini & Brunoni, 1971; Asher & Murtaugh, 1983). The initial protein relaxation is found to be endothermic by 21 kcal/mol, which would mean at most a few kilocalories are stored in the protein structure of myoglobin and released upon relaxation to the deoxy structure. The maximum barrier to CO recombination imposed by the protein relaxation would be approximately 3 kcal/mol, which is in good agreement with the temperature-dependent studies of the kinetics for geminate CO recombination (Frauenfelder et al., 1991; Ansari et al., 1985). The dynamics for the energy relaxation are equally important. Within the signal to noise ratio and including acoustic attenuation, the protein relaxes energetically in less than 200 ps, i.e., no phase delay is observed in the thermal acoustic wave between deoxy and carboxy species which would be observed if energy deposition occurred on longer scales (Genberg et al., 1989). The energetics are essentially identical to the calorimetric determinations of the enthalpy for the formation of MbCO, which has a reported values of 21.4 ± 0.3 kcal/mol (Keyes et al., 1971). This thermodynamic values includes the Fe–CO bond enthalpy and the amount of energy needed to change the protein structure to the fully relaxed deoxy structure. The close agreement between the measured energetics and the thermodynamic value suggests that the driving force for the deoxy tertiary structural changes is essentially exhausted in less than 200 ps.

The time resolution for the thermal grating dynamics, as discussed above, is determined by the grating fringe spacing due to speed of sound limitations imposed on the thermal expansion process. The time resolution to the energetics can be improved by an order of magnitude by going to narrower fringe spacings, and such studies are currently in progress. Within the present time resolution, the dynamics of the structural relaxation are consistent with the concept of a collective mode response. Better time resolution is needed to determine whether there are any energetically significant conformational substates along the structural relaxation pathway for intermediate times, between 30 and 200 ps. There appear to be no significant conformational intermediates past the first few 100 ps for times ranging from 100 ps to 10 ns. There may be slower relaxation components on longer time scales. However, these relaxation processes will be complicated by CO diffusion in the protein and geminate CO recombination which will also lead to energy relaxation processes unrelated to the ligated to unligated tertiary structural changes induced by the doming of the heme.

These results should be compared to time-resolved photoacoustic studies of the protein energetics for myoglobin. The work of Leung et al. (1987) found energetics that were attributed to an Fe–CO bond enthalpy of 13 kcal/mol. Similar studies by Westrick et al. (1987, 1990) have found energetics that depend on the type of heme protein and vary from 10 kcal/mol to nearly exothermic processes for different relaxation components. The variations in energetics in this latter study were believed to arise from solvation effects associated with the breaking of the arginine proponiate salt bridge at the protein's surface. The total change in enthalpy was on the order of 14 kcal/mol. The energetics reported in the present study do not agree with these studies. However, it must be borne in mind that the photoacoustic studies are sensitive to times that are similar to the diffusion time of CO out of the protein. The piezoelectric transducers (acoustic detectors) used in these studies have frequency bandwidths that cover primarily relaxation processes from 100 ns to 10 μs. The diffusion of CO out of the protein is occurring on the 100-ns time scale (Gibson et al., 1986), i.e., within the dynamic window sampled by photoacoustic measurements. Once the CO escapes the protein, the protein energetics will be lowered by the aqueous solvation of the CO [approximately 3 kcal/mol (Leung et al., 1987)] and by an increase in the interactions between residues that were disrupted by the presence of the ligated (E_{T_2} in Figure 7). This latter energy involves relaxation of the protein structure but is distinct from the tertiary structural changes driven by the doming of the heme. The photoacoustic studies may have additional contributions from CO diffusion within the protein, aqueous solvation of the CO, and small contributions from CO recombination. In contrast, the phase grating is determining the energetics on time scales much faster than either CO diffusion out of the protein or geminate CO recombination. In this case, the energetics should only reflect the protein relaxation associated with the tertiary structural changes induced by CO photodissociation and the Fe–CO bond enthalpy. The fact that the grating and photoacoustic measurements do not agree most likely reflects that the two different approaches are measuring different phases of the protein relaxation. On the basis of the better time resolution of the grating relative to the photoacoustic studies, the thermal phase grating approach is expected to give a more accurate determination of the energetics of the initial relaxation processes.

In the MbCO studies, the energetics of the initial protein relaxation are virtually identical to the Fe–CO bond enthalpy. This result means that there is very little energy stored in the protein structure. The surrounding globin acts like an elastic basket for the prosthetic heme group. In contrast to the myoglobin studies, HbCO contains a significant amount of energy stored in the protein structure. This energy is released upon CO photodissociation and increases the amplitude of the thermal grating component over that observed for MbCO. This observation is evident in the data shown in Figure 8 in which the thermal grating response is much larger for HbCO and MbCO. Again, there was observed a fast relaxation component of less than 200 ps with no significant slower relaxation components. The amplitude of this energy relaxation component corresponded to 43 ± 3 kcal/mol or a difference of 11 ± 3 kcal/mol of stored energy in the Hb:CO protein system. We encountered problems with light scatter in the HbCO glycerol/water system which limited the precision of the measurements and is the source of the larger error bar for the HbCO measurements relative to the MbCO studies. Nevertheless, it is clear that there is significantly more energy released into the bath during the structural relaxation of hemoglobin.

As in the case of myoglobin, it is interesting that the amount of energy involved in the initial tertiary relaxation of hemoglobin is very close to the thermodynamic values. Previous determinations of the enthalpy change from the fully relaxed deoxy-Hb to fully ligated Hb found enthalpy changes of approximately 13–15 kcal/mol (Keyes et al., 1971; Mills et al., 1979). These values are close to the measured value of 11 ± 3 kcal/mol. It appears that most of the driving force for the tertiary structural changes is relieved in less than 200 ps. It is the tertiary structural changes that affect the quaternary structure force balance at the $\alpha\beta$ subunit interface. From the energetics, it appears that the tertiary structure changes have also accessed the stored strain energy in the

quaternary structure on a very fast time scale. This is an interesting finding. If the collective mode response is found to be the dominant mechanism for propagation of the tertiary conformational changes, then the difference in energetics associated with the quaternary structure involves a relaxation in structure redistributed over many atomic degrees of freedom. In this event, the energy of cooperativity involved in the allosteric control of hemoglobin is best described within the distributed energy model of Hopfield rather than stored in specific regions in the protein structure (Hopfield, 1973). However, before this evidence for quaternary structure effects can be taken as conclusive, the overall energetics need to be further studied using isolated subunits rather than myoglobin as a reference. Such studies would eliminate potential complications from tertiary structural differences in fully assessing the effect of the quaternary structure on the energetics.

Concluding Remarks. For both MbCO and HbCO, the grating studies indicate that the global relaxation following CO dissociation is occurring on a 10-ps time scale or less. Raman studies of the proximal histidine motion find that protein motion near the heme is occurring within this same time frame. The close correspondence in dynamics of the global coordinate to structural changes in proximity to the heme focal point give a correlation of the motion over two length scales. This correlation and the observed dynamics for the acoustic changes in the protein strain provide evidence that the initial structural changes involve segmental motion, i.e., coupling to a superposition of collective modes of the protein. The collective displacement of atoms is the most efficient mechanism possible for propagating the structural changes. This mechanism is distinct from either the localized strain model or the conformational substate model in that the forces are extensively distributed and the motion occurs in phase without sampling of intermediates. Within the context of this model, better time resolution for the relaxation of the global structural coordinate and proximal histidine is needed to determine whether or not a 1:1 correlation exists and to determine the degree of coupling of the heme site to collective modes of the protein.

The above observations do not rule out conformational substates playing a role in propogating the structural changes. Recent evidence from time-resolved circular dichroism (Xie & Simon, 1990) has found slower relaxation processes occurring on a hundred picosecond time scale for myoglobin at room temperature, which is indicative of conformational substates along the reaction coordinate. The grating also detects small-amplitude relaxation processes occurring on nanosecond time scales at lower temperatures. The main observation is that most of the relaxation in acoustic strain occurs during the initially rapid response of the protein to ligand dissociation. This finding is similar to optical and Raman studies of MbCO, which, to date, have found an initially rapid relaxation phase in which most or all of the detectable changes in tertiary structure, with respect to the observable, occur within the first few picoseconds (Petrich et al., 1989; Freidman et al., 1985). The grating studies indicate that the dominant phase of the relaxation is this initially rapid relaxation phase, which has been implicated to occur through coupling to collective modes. This feature of the relaxation is important, as the collective phase of the atomic displacements would minimize the total conformational phase space sampled by the protein as it relaxes toward its final global energy minimum.

The energetics of the different phases of protein motion can be used as a criterion for determining the dominant mechanism for the structural changes and in elucidating the relative importance of various phases of the protein's structural relaxation. For both myoglobin and hemoglobin, the measured energetics are fairly close to thermodynamic measurements. This observation and the lack of any significant slow relaxation components (>200 ps) suggest that the protein relaxation is *energetically* complete on a 100-ps time scale or less. The extremely fast time scale for the release of the stored strain energy and structural relaxation is an important consideration. If the difference in energetics can be definitely assigned to quaternary effects, these findings would mean that tertiary relaxation at the subunit level almost immediately affects the quaternary interfacial force balance. Time averaged, the heme protein subunits energetically exist primarily in either the oxy or deoxy tertiary state. This result would help rationalize how a simple two-state model for allosteric control can account for most of the cooperative effects in hemoglobin (Monod et al., 1965; Shulman et al., 1975). In addition, the observed volume changes and corresponding energetics provide a simple framework to view the communication pathway between the subunits.

To resolve the above issues regarding energetics, the dynamic range of the thermal grating can be extended from picosecond to millisecond time scale with changes in beam geometries. It will be very interesting to extend these studies to the microsecond range to follow the R to T quaternary structural changes and make a complete connection with the thermodynamic and photoacoustic measurements. Numerous questions can be answered regarding the cumulative effect of ligand loss on the energetics and the driving forces for the R to T switch for O_2 affinity. In this regard, the grating provides a direct determination of the protein strain and released energy. The combined ability to measure the dynamics of the global motion and energetics over a wide dynamic range makes this technique an important new probe of protein dynamics.

ACKNOWLEDGMENT

We thank Professor George McLendon for help in the heme protein preparations.

REFERENCES

Anfinrud, P. A., Han, C., & Hochstrasser, R. M. (1989) *Proc. Natl. Acad. Sci. U.S.A 86*, 8387.

Ansari, A., Berendzen, J., Bowne, S. F., Frauenfelder, H., Iben, I. E. T., Sauke, T. B., Shyamsunder, E., & Young, R. D. (1985) *Proc. Natl. Acad. Sci. U.S.A. 82*, 5000.

Antonini, E., & Brunori, M. (1971) in *Hemoglobin and Myoglobin in Their Reactions with Ligands*, North-Holland Publishing, Amsterdam.

Asher, S. A., & Murtaugh, J. (1983) *J. Am. Chem. Soc. 105*, 7244.

Austin, R. H., Beeson, K. W., Eisenstein, L., Frauenfelder, H., & Gunsalus, I. C. (1975) *Biochemistry 14*, 5355.

Brooks, B., & Karplus, M. (1985) *Proc. Natl. Acad. Sci. U.S.A. 82*, 4995.

Chan, C. K., & Page, J. B. (1983) *J. Chem. Phys. 79*, 5234.

Cho, G. C., Kütt, W., & Kurz, H. (1990) *Phys. Rev. Lett. 65*, 764.

Cusack, S., & Doster, W. (1990) *Biophys. J. 58*, 243.

Dharamsi, A. N., & Hassam, A. B. (1989) *J. Acoust. Soc. Am. 85*, 1560.

Eaton, W. A., Hanson, L. K., Stephens, P. J., Sutherland, J. C., & Dunn, J. B. R. (1978) *J. Am. Chem. Soc. 100*, 4991.

Eichler, H. J., Gunter, P., & Pohl, D. W. (1986) in *Laser-Induced Dynamic Gratings*, Springer-Verlag, Berlin.

Elber, R., & Karplus, M. (1987) *Science 235*, 318.
Findsen, E. W., Friedman, J. M., Ondrias, M. R., & Simon, S. R. (1985a) *Science 229*, 661.
Findsen, E. W., Scott, T. W., Chance, M. R., Friedman, J. M., Ondrias, M. R. (1985b) *J. Am. Chem. Soc. 107*, 3355.
Frauenfelder, H., Sligar, S. G., & Wolynes, P. G. (1991) *Science, 254*, 1598.
Friedman, J. M., Scott, T. W., Fisanick, G. J., Simon, S. R., Findsen, E. W., Ondrias, M. R., & MacDonald, V. W. (1985) *Science 229*, 187.
Gelin, B. R., & Karplus, M. (1977) *Proc. Natl. Acad. Sci. U.S.A. 74*, 801.
Genberg, L. (1990) Ph.D. Thesis, University of Rochester, Rochester, NY.
Genberg, L., Heisel, F., McLendon, G., & Miller, R. J. D. (1987) *J. Phys. Chem. 91, 5521.*
Genberg, L., Bao, Q., Gracewski, S., & Miller, R. J. D. (1989) *Chem. Phys. 131*, 81.
Genberg, L., Richard, L., McLendon, G., & Miller, R. J. D. (1991) *Science 251*, 1051.
Gibson, Q. H., & Ainsworth, S. (1957) *Nature 180*, 1416.
Gibson, Q. H., Olson, J. S., McKinnie, R. E., & Rohlfs, R. J. (1986) *J. Biol. Chem. 261*, 228.
Greene, B. I., Hochstrasser, R. M., Weisman, R. B., & Eaton, W. A. (1978) *Proc. Natl. Acad. Sci. U.S.A. 75*, 5255.
Henry, E. R., Sommer, J. H., Hofrichter, J., & Eaton, W. A. (1983) *J. Mol. Biol. 166*, 443.
Hopfield, J. J. (1973) *J. Mol. Biol. 77*, 207.
Huppert, D., Straub, K. D., & Rentzepis, P. M. (1977) *Proc. Natl. Acad. Sci. U.S.A. 74*, 4139.
Keyes, M. H., Falley, M., & Lumry, R. J. (1971) *J. Am. Chem. Soc. 93*, 2035.
Kogelnik, H. (1969) *Bell Syst. Tech. J. 48*, 2909.
Kraehenbuhl, J. P., Galardy, R. E., & Jamieson, J. D. (1974) *J. Exp. Med. 139*, 208.
Leone, M., Cupane, A., Vitrano, E., & Cordone, L. (1987) *Biopolymers 26*, 1769.
Leung, W. P., Cho, K. C., Chau, S. K., & Choy, C. L. (1987) *Chem. Phys. Lett. 141*, 220.
Lingle, R., Xu, X. B., Zhu, H. P., Yu, S. C., Hopkins, J. B., & Straub, K. D. (1991) *J. Am. Chem. Soc. 113*, 3992.
Martin, J. L., Migus, A., Poyart, C., Lecarpentier, Y., Astier, R., & Antonetti, A. (1983) *Proc. Natl. Acad. Sci. U.S.A. 80*, 173.
Miller, R. J. D. (1991) *Annu. Rev. Phys. Chem. 42*, 581.
Miller, R. J. D., Pierre, M., Rose, T., & Fayer, M. D. (1984) *J. Phys. Chem. 80*, 3021.
Miller, R. J. D., Deak, J., Palese, S., Pereira, M., Richard, L., & Schilling, L. (1992) *Ultrafast Phenomena 8* (Martin, J. L., Ed.) Springer-Verlag, Heidelberg.
Mills, F. C., Ackers, G. K., Gaud, H. T., & Gill, S. J. (1979) *J. Biol. Chem. 254*, 2875.
Min, L., & Miller, R. J. D. (1989) *Chem. Phys. Lett. 163*, 55.
Min, L., & Miller, R. J. D. (1990) *Appl. Phys. Lett. 56*, 524.
Monod, J., Wyman, J., & Changeux, J. P. (1965) *J. Mol. Biol. 12*, 88.
Murray, L. P., Hofrichter, J., Henry, E. R., & Eaton, W. A. (1988a) *Biophys. Chem. 29*, 63.
Murray, L. P., Hofrichter, J., Henry, E. R., Ikeda-Saito, M., Kitagishi, K., Yonetani, T., & Eaton, W. A. (1988b) *Proc. Natl. Acad. Sci. U.S.A. 85*, 2151.
Nelson, K. A., & Fayer, M. D. (1980) *J. Chem. Phys. 72*, 5202.
Nelson, K. A., Casalegno, R., Miller, R. J. D., & Fayer, M. D. (1982a) *J. Chem. Phys. 77*, 1144.
Nelson, K. A., Miller, R. J. D., Lutz, D., & Fayer, M. D. (1982b) *Appl. Phys. Lett. 53*, 1144.
Painter, P. C., Mosher, L. E., & Rhoads, C. (1982) *Biopolymers 21*, 1469.
Perutz, M. F. (1970) *Nature 228*, 726.
Perutz, M. F., Fermi, G., Luisi, B., Shannan, B., & Liddington, R. C. (1987) *Acc. Chem. Res. 20*, 309.
Petrich, J. W., & Martin, J. L. (1989) *Chem. Phys. 131*, 31.
Petrich, J. W., & Martin, J. L., Houde, D., Poyart, C., & Orszag, A. (1987) *Biochemistry 26*, 7914.
Petrich, J. W., Poyart, C., & Martin, J. L. (1988) *Biochemistry 27*, 4049.
Siegman, A. E. (1977) *J. Opt. Soc. Am. 67*, 545.
Seno, Y., & Gō, N. (1990) *J. Mol. Biol. 216*, 111.
Shulman, R. G., Hopfield, J. J., & Ogawa, S. (1975) *Q. Rev. Biophys. 8*, 325.
Westrick, J. A., Goodman, J. L., & Peters, K. S. (1987) *Biochemistry 26*, 8313.
Westrick, J. A., Peters, K. S., Ropp, J. D., & Sligar, S. G. (1990) *Biochemistry 29*, 6741.
Xie, X. L., & Simon, J. D. (1991) *Biochemistry 30*, 3682.